Results & Discussion

Chapter IV

Experimental Results And Discussion

4.1 Introduction

In this chapter , the results of the various experimental work which were described in chapter III are presented. Section 4.2 gives the characterisation results of the crystalline material. In this section the structural, optical and electrical characterisation results for crystalline-Si and crystalline-Ge are discussed. The x-ray diffraction results for crystalline-Si are presented in section 4.2.1, followed by the optical characterisation results presented in section 4.2.2. Results of the Hall effect and the four probe measurements for crystalline - Ge and a.c. and d.c. conductivity measurements for crystalline-Si are presented in section 4.2.3. The results obtained on the structural, optical and electrical characterisation of hydrogenated amorphous silicon (a-Si:H) for various flow rates and various annealing temperatures are presented in section 4.3. The preparation conditions of the a-Si:H studied in this work are presented in section 4.3.1. The Fourier Transform Infra-Red spectroscopy (FTIR) results are presented for a-Si:H annealed at different temperatures are presented in section 4.3.2. X-ray diffraction results for these samples are presented and discussed in detail in section 4.3.3, followed by the optical characterisation results in section 4.3.4. The electrical a.c. and d.c. conductivity measurement results for these samples are presented in section 4.3.5.

4.2 Characterisation Results For The Crystalline Materials

4.2.1 Structural Characterisation Results For Crystalline-Si

In the experiment , the structural investigation for crystalline Si has been obtained by taking its x-ray diffractograms. This sample was scanned in the range of $10^0 < 2\theta < 70^0$ and the x-ray diffractogram of the sample has been illustrated in fig. 4.1. The peak which was obtained in the result corresponds to <400> plane orientation. For this crystalline Si sample, a prominent sharp peak was observed at $2\theta = 69.20^0$. This sharp peak in the x-ray diffractogram indicate that the sample is crystalline in nature.

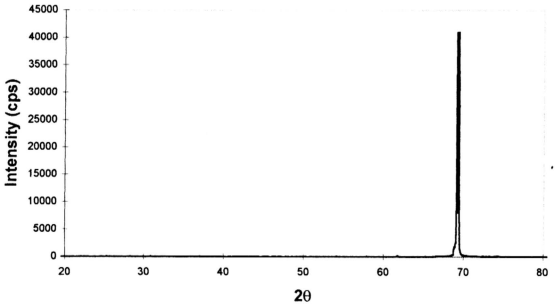

Figure 4.1 : The x-ray diffractogram of the crystalline silicon wafer

4.2.2 Optical Characterisation Results For Crystalline Si

The optical characterisation for crystalline-Si was carried out by taking its transmission spectrum. This was done by scanning the sample in the range of 300 nm - 3000 nm by using the Shimadzu UV-VIS double beam spectrometer model and the spectrum which was obtained in the experiment has been plotted in fig. 4.2. From this transmission spectrum, the refractive index , the absorption coefficient and the absorption constant were calculated and the results are analysed in the chapter V.

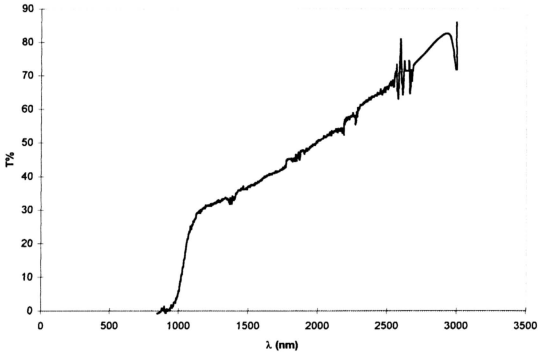

Figure 4.2 : The optical transmission spectrum of the crystalline silicon wafer

4.2.3. Electrical Characterisation Results For Crystalline Ge and Crystalline Si

I) Four Probe Method

By using this method , the $\log_{10}(\rho)$ versus 1/T relationship of crystalline-Ge was studied , where ρ is the resistivity of the sample and T is the absolute temperature. In this experiment, the temperature of the sample has been increased from 302.16^0 K to 453.16^0 K. This measurement was carried out for the crystalline-Ge sample which had conducting and non-conducting bases. Tables 4.1 and 4 .2 provides the experimental results for the crystalline Ge for both conducting and non-conducting bases. Table 4.3 presents the calculated energy gap of the crystalline Ge. The calculated variation of resistivity with increase in temperature has been plotted as a graph of $\log_{10}(\rho)$ versus 1/T for both conducting and non-conducting bases. These have been presented in figure 4.3 and figure 4.4.

T^0C	Voltage ± 1 (mV)	T^0 K	$\rho_0 \pm 0.001$ (ohm.cm)	$\rho \pm 0.001$ (ohm.cm)	$T^{-1} \times 10^{-3}$	$\log_{10}(\rho)$ ± 0.001
28	242	302.16	60.742	5406.038	3.31	3.733
40	198	313.16	49.698	4423.122	3.19	3.646
50	170	323.16	42.670	3797.63	3.09	3.580
60	145	333.16	36.395	3239.155	3.00	3.510
70	121	343.16	30.371	2703.19	2.91	3.432
80	102	353.16	25.602	2278.578	2.83	3.358
90	87	363.16	21.837	1943.493	2.75	3.289
100	72	373.16	18.122	1612.858	2.68	3.208
110	59	383.16	14.834	1320.226	2.61	3.121
120	49	393.16	12.274	1092.386	2.54	3.038
130	38	403.16	9.638	857.782	2.48	2.933
140	29	413.16	7.204	641.156	2.42	2.807
150	22	423.16	5.522	491.458	2.36	2.691
160	16	433.16	4.066	361.874	2.31	2.559

Table 4.1 : Experimental results for crystalline-Ge with conducting base.

T^0C	Voltage ± 1 (mV)	T^0 K	$\rho_0 \pm 0.001$ (ohm.cm)	$\rho \pm 0.001$ (ohm.cm)	$T^{-1} \times 10^{-3}$	$\log_{10}(\rho)$ ± 0.001
28	324	302.16	81.324	41.638	3.31	1.619
40	318	313.16	79.818	40.867	3.19	1.611
50	293	323.16	73.543	37.654	3.09	1.576
60	249	333.16	62.499	31.999	3.00	1.505
70	199	343.16	49.949	25.574	2.91	1.408
80	150	353.16	37.650	19.277	2.83	1.285
90	112	363.16	28.122	14.393	2.75	1.158
100	83	373.16	20.833	10.666	2.68	1.028
110	61	383.16	15.311	7.839	2.61	0.894
120	45	393.16	11.295	5.783	2.54	0.762
130	34	403.16	8.534	4.369	2.48	0.640
140	26	413.16	6.526	3.341	2.42	0.524
150	19	423.16	4.769	2.442	2.36	0.388
160	15	433.16	3.765	1.928	2.31	0.285

Table 4.2 : Experimental results for crystalline-Ge with non- conducting base.

Types of sample	Energy gap of the sample ± 0.02
conducting base sample	0.68 eV
non-conducting base sample	0.75 eV

Table 4.3 : Energy gap of the crystalline-Ge for conducting and non-conducting base

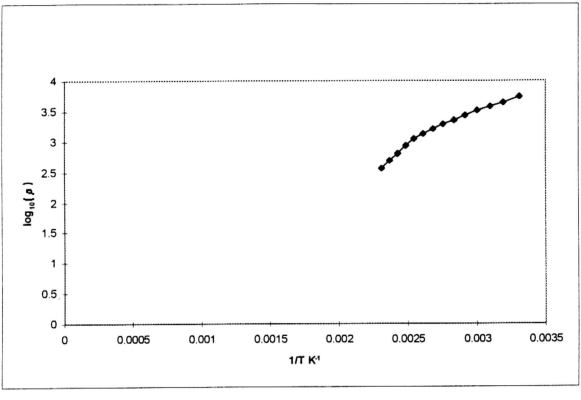

Figure 4.3 : The variation of log(ρ) with temperature inverse for crystalline Germanium with conducting base

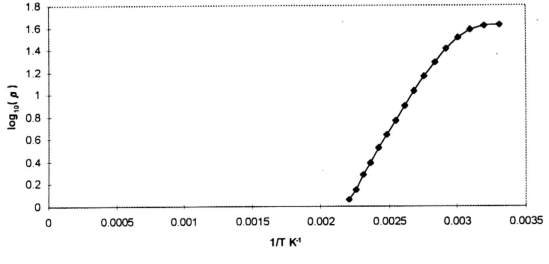

Figure 4.4: The variation of log(ρ) with temperature inverse for crystalline Germanium with non-conducting base

II) D.C. Conductivity Measurement

This measurement was carried out for crystalline-Si by depositing aluminium electrodes in the transverse configuration on the sample (fig. 3.15) and the measurement was carried out by using Keithly Source Measurement unit as explained in chapter III. In this experiment, the temperature of the sample was increased from 297^0K to 338^0K. The variation of $\log_{10}(\rho)$ with inverse temperature (1/T) was studied and the corresponding data are plotted in fig. 4.5. Fig. 4.6 illustrates the variation of voltage with current for the temperature range of 297^0K to 338^0K for the crystalline Si.

III) Hall Effect Measurement

This measurement was carried out for p-type and n-type crystalline Ge. The measurement has been carried out by using Hall measurement set-up which was discussed in chapter III. In the experiment, the Hall voltages for both directions of current and magnetic field were measured for both types of samples (n-type and p-type) as a function of the current keeping the magnetic field constant. The variation of the measured Hall voltage with the applied current has been plotted in fig. 4.7 and fig. 4.8. The Hall voltage as function of magnetic field keeping the current constant at a suitable value is also measured for both the samples in the experiment and the variation of Hall voltage as a function of magnetic field has been plotted in fig. 4.9 and fig. 4.10. From the graph of Hall voltage as a function of the magnetic field, the parameters which can be calculated are the Hall Coefficient, the charge carrier density and the carrier mobility.

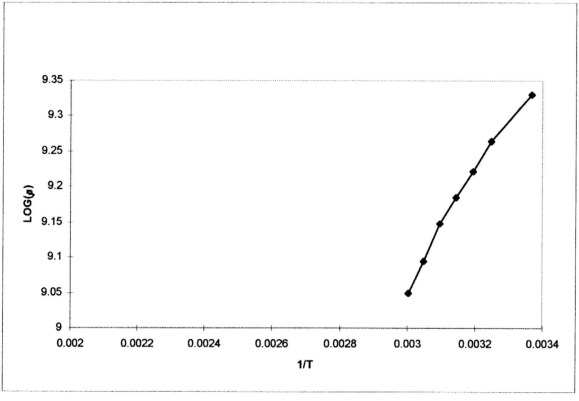

Figure 4.5 : The variation of log(ρ) with temperature inverse for crystalline silicon

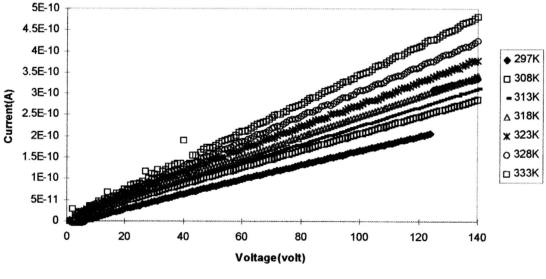

Figure 4.6: The variation of voltage as a function with current for various temperature range for crystalline Silicon

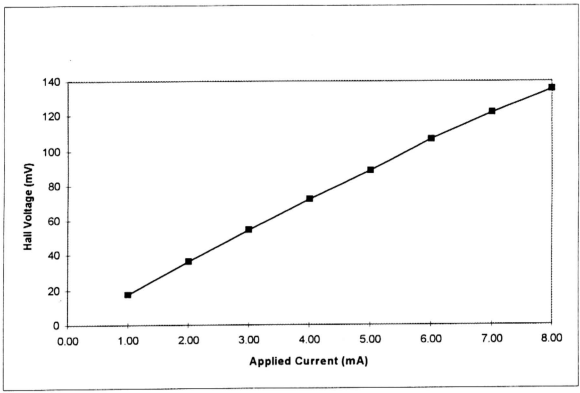

Figure 4.7: Variation of Hall voltage as a function of current for n-type Germanium

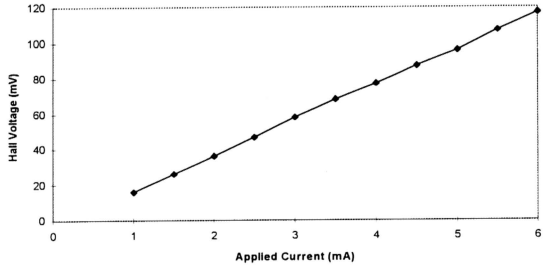

Figure 4.8: Variation of Hall voltage as a function of current for p-type Germanium

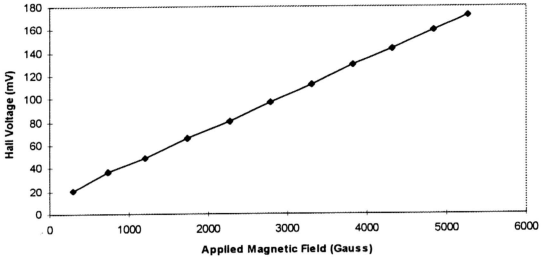

Figure 4.9: Variation of Hall voltage as a function of magnetic field for n-type Germanium

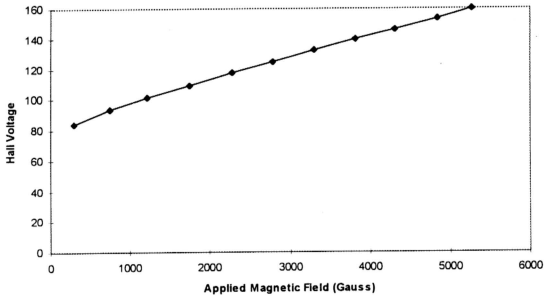

Figure 4.10: Variation of Hall voltage as a function of magnetic field for p-type Germanium

IV) A.C. Conductivity Measurement

The a.c. conductivity measurement for crystalline-Si was carried out by depositing aluminium electrodes in the transverse configuration on the sample (fig. 3.15) and the measurement was carried out for the sample by using Hioki LCR 3520 Bridge. These measurements were performed at room temperature for three different conditions such as before annealing, and after annealing at 300^0C and at 500^0C for the same crystalline Si sample. The results which were obtained for the frequency range between 42 Hz to 5.0 MHz have been presented in graphs for all three different conditions. The parameters which were measured as a function of the frequency were the series capacitance, the parallel capacitance, the loss coefficient and the conductance. These parameters have been plotted as a function of the frequency in fig. 4.11 to fig. 4.14 for all the three conditions for the same sample.

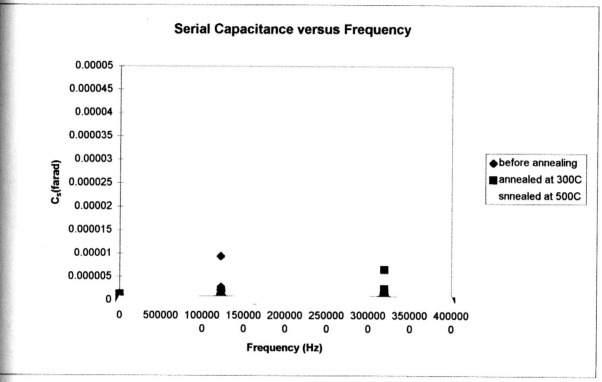

Figure 4.11 : Variation of serial capacitance as a function of frequency for crystalline Si at various annealed temperature

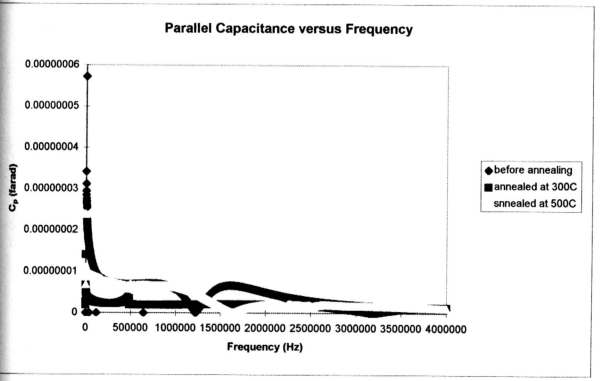

Figure 4.12 : Variation of parallel capacitance as a function of frequency for crystalline Si at various annealed temperature

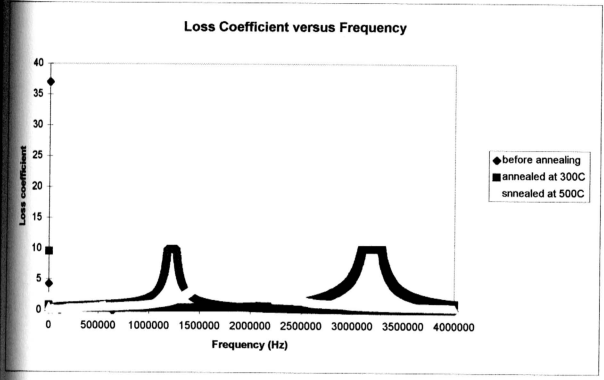

Figure 4.13 : Variation of loss coefficient as a function of frequency for crystalline Si at various annealed *temperature*

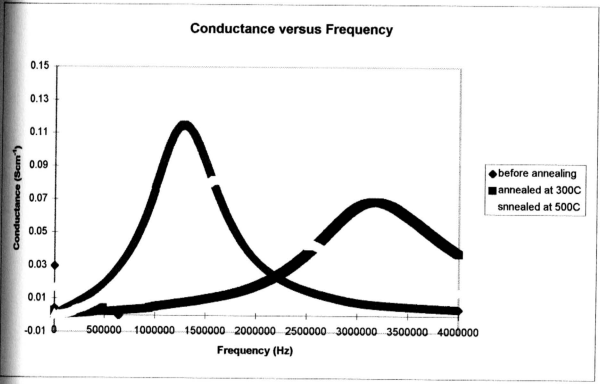

Figure 4.14 : Variation of conductance as a function of frequency for crystalline Si at various annealed *temperature*

4.3. Hydrogenated Amorphous Silicon (a-Si:H)

4.3.1 Preparation condition of a-Si:H

The a-Si:H thin film studied in this work was prepared using a horizontal D.C. plasma glow discharge system. The deposition system was home built and was presented and discussed in chapter III. The films were deposited simultaneously on crystalline silicon and soda lime glass substrates. The films on crystalline silicon substrate were used for infra-red analysis while on glass substrate were used for optical spectroscopy, x-ray diffraction, alternating current and direct current conductivity measurement studies. Two sets of a-Si:H films were investigated. The silane gas (SiH_4) flow-rate was fixed at 5 sccm and 25 sccm to produce these samples. The deposition pressure was maintained at 0.8 mbar for both samples. The ionisation current was fixed at 12 mA and to maintain the current, the voltage was fixed at 500 volt. The base pressure prior to deposition was 4.2×10^{-2} mbar.

Generally, the deposition rate of the sample prepared using a silane flow-rate of 5 sccm (5 sccm sample) was lower than the sample prepared using a silane flow-rate of 25 sccm (25 sccm sample) regardless whether the sample was on glass or crystalline silicon substrates. However, for the 5 sccm sample the deposition rate was higher on the glass substrate then on the crystalline silicon substrate. But for the 25 sccm sample a reverse phenomenon was observed, the film was deposited at a faster rate on the crystalline silicon than on the glass substrate. Thus, higher silane flow-rate increased the deposition rate of the film but deposition rate was also observed to be dependent on the substrate used.

Sample	Thickness ± 6 μ(nm)	Deposition Rate±0.09 (nm/min)
5 sccm on glass	725	8.06
25 sccm on glass	1289	14.32
5 sccm on crystalline-Si	422	4.69
25 sccm on crystalline-Si	2470	27.44

Table 4.4 . Variation of thickness with deposition rate for 5 sccm and 25 sccm sample on glass and crystalline-Si substrate.

4.3.2. FTIR Characterisation Results of a-Si:H

The position of the absorption bands observed in the Fourier Transform Infra-Red (FTIR) spectra prepared for the two flow-rates mentioned above and annealed at 300^0C and 500^0C are presented in tables 4.5 and 4.6. The corresponding spectra are shown in figures 4.15 and 4.16 with the absorption peaks marked.

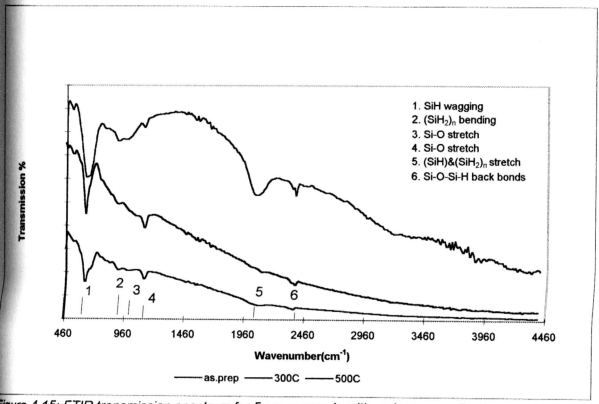

Figure 4.15: FTIR transmission spectrum for 5 sccm sample with various annealing temperature.

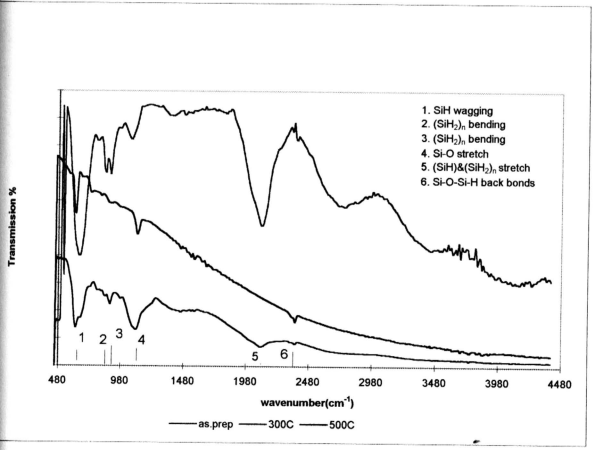

Figure 4.16: FTIR transmission spectrum for 25 sccm sample with various annealing temperature

Absorption peak from literature(cm^{-1})	as prepared cm^{-1}	annealed at 300°C cm^{-1}	annealed at 500°C cm^{-1}	assignment of the absorption peak
640 [73-75]	618	611	619	SiH wagging
2000 & 2100 [73,74,76-78]	2034	2025	not observed	(SiH)&(SiH_2) stretch
890 [79-83]	890	890	898	$(SiH_2)_n$ bending
940 [79-83]	974	not observed	not observed	Si-O stretch
1100 [79-83]	1120	1114	1114	Si-O stretch
2364 [84]	2362	2362	2362	Si-O-Si-H

Table 4.5 : Absorption peaks observed from the FTIR spectra for the 5 sccm sample, as-prepared and annealed at temperatures of 300°C and 500°C.

Absorption peak from literature(cm^{-1})	as prepared cm^{-1}	annealed at 300°C cm^{-1}	annealed at 500°C cm^{-1}	assignment of the absorption peak
640 [73-75]	620	626	610	SiH wagging
2000 & 2100 [73,74,76-78]	2104	2104	not observed	(SiH)&(SiH_2) stretch
850 [79-83]	856	not observed	not observed	$(SiH_2)_n$ bending
890 [79-83]	904	890	884	$(SiH_2)_n$ bending
1100 [79-83]	1064	1106	1114	Si-O stretch
2364 [84]	not observed	2370	2370	Si-O-Si-H

Table 4.6 : Absorption peaks observed in the FTIR spectra for the 25 sccm sample, as-prepared and annealed at temperatures of 300°C and 500°C.

The spectra for both a-Si:H samples exhibit two prominent absorption bands at 640 cm^{-1} and 2064 cm^{-1}. The former absorption peak corresponds to Si-H wagging mode while the latter is due to the superposition of absorption modes at 2000 cm^{-1} and 2100 cm^{-1} which correspond to the Si-H and Si-H_2 stretching modes respectively. For a-Si:H films, the main region of interest lies between 1800 cm^{-1} and 2200 cm^{-1} silicon-hydrogen stretching vibration bands. The profiles of these absorption bands are sensitive to the flow-rates where due to

the changes in the silane concentration, the profiles of the silicon hydrogen stretching vibrations were found to change. For the 5 sccm sample, the silicon-hydrogen stretching band was observed at 2034 cm^{-1} and this indicated that the sample had more hydrogen bonded as monohydrides. For the 25 sccm the silicon-hydrogen absorption band shifted to higher wavenumber at 2104 cm^{-1}, indicating that the sample had more hydrogen bonded as polyhydride [73,74,76-78]. For the 25 sccm as prepared sample, the absorption bands at 620 cm^{-1} which corresponded to the Si-H wagging mode was found to be broader and higher in intensity as compared to the 5 sccm sample. This observation indicated that the amount of hydrogen atom incorporated into the 25 sccm as prepared sample was comparatively larger than the 5 sccm as prepared sample. For 5 sccm as prepared sample, the Si-H wagging mode was observed at 618 cm^{-1} and two absorption bands at 890 cm^{-1} and 974 cm^{-1} were observed corresponding to the $(SiH_2)_n$ bending modes and Si-O stretching modes respectively. For the 25 sccm as prepared sample, the Si-H wagging band shifted to 626 cm^{-1}. The $(SiH_2)_n$ bending modes for the 25 sccm sample were observed to be split at 856 cm^{-1} and 904 cm^{-1} and the Si-H stretching mode shifted to 2104 cm^{-1}. This suggested that the 25 sccm sample had microcrystallite structures present [73-75]. The presence of oxygen contamination was indicated by absorption peaks at 974 cm^{-1} and 1120 cm^{-1} in 5 sccm sample and at 1064 cm^{-1} in the 25 sccm sample. The above mentioned absorption bands correspond to silicon-oxygen stretching mode and the intensity, position and profile of the bands are dependent on the silicon to oxygen stoichiometry and vary with the deposition conditions [79-83]. For the 5 sccm sample, the absorption band for the Si-H stretching mode decreased in intensity when the sample was annealed at 300^0C and disappears when the sample was annealed at 500^0C. When the 5 sccm sample was annealed

at 300^{0}C, silicon-hydrogen stretching band shifted towards lower wavenumber indicating that the monohydride bonds in the sample had become more dominant. The disappearance of this absorption band was observed when the sample was annealed at 500^{0}C indicating that the hydrogen evolution had taken place. For 25sccm sample, the absorption band of the silicon-hydrogen stretching at 2104 cm^{-1} also decreased in intensity when the sample was annealed at 300^{0}C and disappears when the sample was annealed at 500^{0}C. When the 25 sccm sample was annealed at 300^{0}C, silicon-hydrogen stretching bond remained stationary indicating that polyhydride bonds were more dominant even when annealed at this temperature. The decrease in intensity indicated that hydrogen was evolved or these bonds were either transformed into other bonds As the sample was annealed at 500^{0}C, the silicon-hydrogen stretching absorption band disappears, indicating that more hydrogen was evolved or transformed into other bonding structures.

For 5 sccm sample, the absorption band corresponding to the SiH wagging mode shifted to 611 cm^{-1} from 618 cm^{-1} when the sample was annealed at 300^{0}C. This absorption band shifted to 619 cm^{-1} when the sample was annealed at 500^{0}C. For the 25 sccm sample, the absorption band was observed to shift to 626 cm^{-1} when annealed at 300^{0}C and when annealed at 500^{0}C, this absorption band shifted to 610 cm^{-1}. For both these samples, the absorption bands corresponding to the SiH wagging mode decreased in intensity when the sample was annealed at 300^{0}C and 500^{0}C. The decrease in the intensity of these absorption peaks as the samples were annealed at 300^{0}C suggested that hydrogen evolved from weakly bonded hydrogen atoms. These weaker Si-H bonds are in the form of $Si{\equiv}H_3$ and $(Si\text{-}H_2)_n$ bonds and suggested by Biegelson et.al [77] are surface bonds. The decrease in the intensity of the Si-H wagging bands when annealed at 500^{0}C suggested that the hydrogen was

evolved either from the stronger bonded hydrogen atoms such as Si-H or $Si{=}H_2$ at the surface, or from $Si{\equiv}H_3$ and $(Si\text{-}H_2)_n$ sites in the bulk. The decrease in the intensity of this band also suggested that the Si-H bonds could also be transformed into Si-O-Si-H bond when annealed at this temperature.

From the transmission spectra, the Si-O stretching bands observed for the 5 sccm sample was observed at 974 cm^{-1} and 1120 cm^{-1}. When annealed at 300^0C, the absorption band at 974 cm^{-1} disappears. The Si-O bonds represented by the absorption band were weakly bonded as indicated by the wave number and were evolved or transformed into the stronger SiO stretching bonds represented by the 1114 cm^{-1} absorption bonds. The absorption band at 1114 cm^{-1} was observed to increase in intensity when annealed at 300^0C. This suggested that indeed the transformation process had taken place. When annealed at 500^0C, the Si-O stretching band decreased in intensity suggesting that oxygen was evolved. For the 25 sccm sample the Si-O stretching band shifted to higher wave number when annealed at 300^0C and 500^0C. The intensity of the absorption peak also was observed to increase when annealed at these temperatures. These suggested the presence of infra-red inactive oxygen in the as prepared sample and when annealed, the oxygen atoms diffused into the bonding structure to form Si-O bond. The shift in the absorption peak towards larger wave numbers confirmed that more oxygen atoms were diffused into the bonding structures making the film less silicon rich.

The effects of annealing at 300^0C and 500^0C on the absorption band within 800cm^{-1} to 900 cm^{-1} which corresponds to SiH_2 and $(SiH_2)_n$ bending scissors configuration[79-83] were also studied. For the 5 sccm as prepared sample this absorption band was observed at 890 cm^{-1} and it remained stationary when the sample was annealed at 300^0C. However,

4.3.3. X-Ray Diffraction Results

Figure 4.17 shows the x-ray diffractogram spectra for the 5 sccm and 25 sccm a-Si:H films studied in this work. Two small Bragg peaks were observed in the spectrum for the 5 sccm film at $2\theta = 13^0$ and 15^0. For the 25 sccm sample, in addition to the two Bragg peaks which were observed in the former samples three more Braggs peaks appeared at $2\theta = 16.18^0$, 37.80^0 and 44.06^0. These peaks indicated that the crystalline structures in these film were like silicon oxide crystal with orthorhombic structure. The peaks at $2\theta = 13.0^0$, 15.0^0, 16.18^0, 37.8^0 and 44.06^0 corresponds to the <200>, <220>, <261> and <222> [66] planes of this structure respectively. The peaks at $2\theta = 15.0^0$ and 16.18^0 both correspond to the <220> planes. Two peaks were observed due to non-chromatic radiation source. The intensity of the <200> and <220> peaks observed in the x-ray diffraction spectrum of 25 sccm sample was higher as compared to the 5 sccm sample. However, the most significant difference observed was the presence of the sharp peak at $2\theta = 44.06^0$ which corresponded to the <222> plane. The preferential orientation of the planes changed when the flow-rate of silane increased from 5 sccm to 25 sccm. The significant increase in the peak intensities observed for the 25 sccm sample, showed that the volume fraction of crystalline material in the 25 sccm sample was larger. The result showed that in both these film, SiO_2 nanocrystals or possibly microcrystal were embedded in the amorphous structure of a-Si:H. Higher silane flow-rates resulted in more oxygen atoms being trapped thus forming the SiO_2 nanocrystals in the film. The oxygen atoms were probably from air or water vapour present in the deposition chamber. Even though this chamber was evacuated prior to deposition, the vacum was not sufficient to evacuate these oxygen atoms.

Figures 4.18 and 4.19 showed the x-ray diffraction spectra for the 5 sccm and 25 sccm as prepared samples and when annealed at 300^0C and 500^0C respectively. The intensity of the peaks corresponding to the <200> plane increased when the 5 sccm sample was annealed at 300^0C. This showed that the volume fraction of crystalline material increased when annealed at this temperature indicating that more nanocrystals are formed. When the sample was annealed at 500^0C, the diffraction peaks totally disappeared. This indicates that the crystalline structure collapsed when annealed at this temperature. The film becomes nearly amorphous. In figure 4.19, it was observed that for the 25 sccm sample, the Bragg peaks corresponding to the <200> and <220> planes reduced in intensity and the peaks corresponding to the <261> and <222> planes disappeared when annealed at 300^0C. The preferential orientation of the planes changed and the volume fraction of crystalline material decreased when annealed at this temperature. However when annealed at 500^0C, the peaks corresponding to the <200> and <220> planes disappeared while the peaks corresponding to the <261> and <222> planes reappeared. The intensity of the peak corresponding to the <222> plane was significantly higher and sharper. This observation showed that the preferential orientation of the planes were again changed and the volume fraction of the crystalline material increased when annealed at 500^0C. The sharp peak also indicates that the crystallite size of this structure was larger but smaller than the as-prepared sample [87]. Thus the effects of annealing on the structure of the film were different for the 5 sccm and the 25 sccm films. The higher silane flow-rate resulted in a higher volume fraction of crystalline material and the formation of larger nanocrystals with <222> plane as the preferential orientation plane. The nanocrystalline structure with this

when annealed at 300°C but was restored when annealed at 500°C but with lower volume fraction of crystalline material.

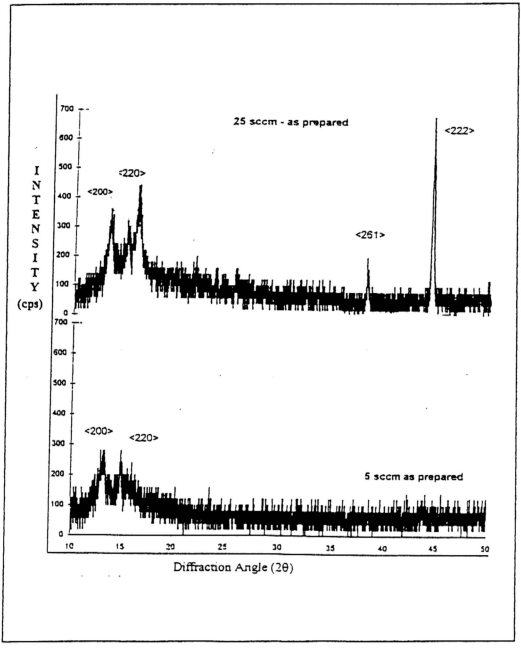

Figure 4.17 : X-ray diffractograms of 5 sccm and 25 sccm as prepared a-Si:H

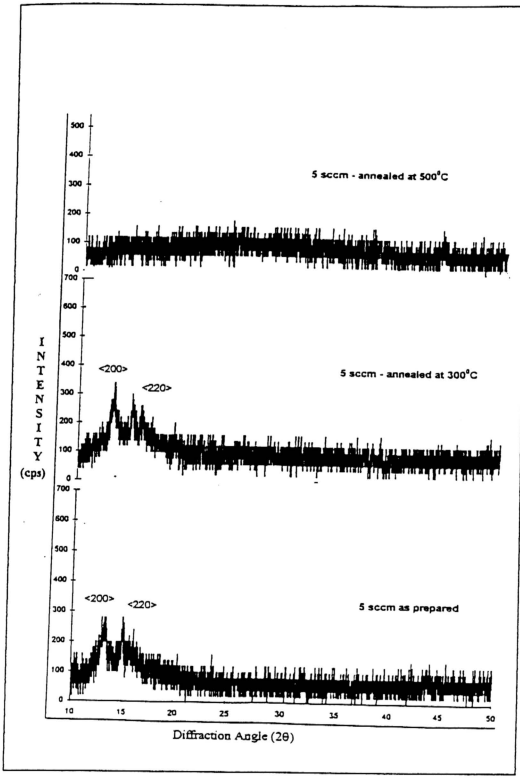

Figure 4.18 : X-ray diffractograms of 5 sccm a-Si:H for different annealing temperatures

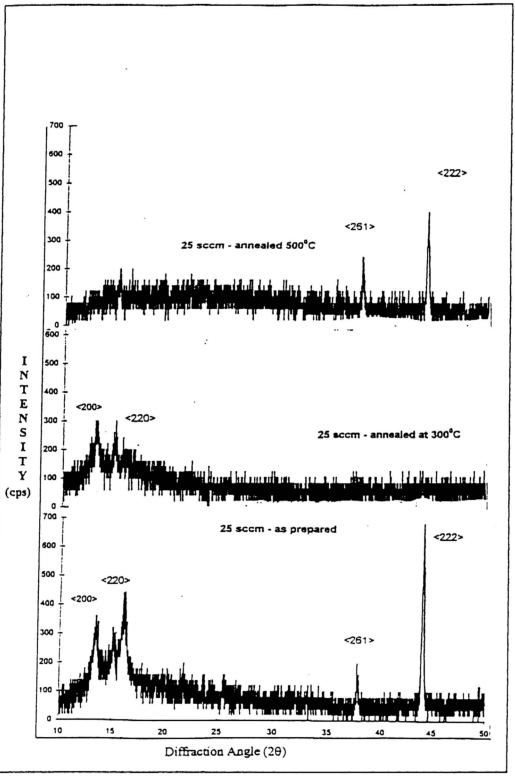

Figure 4.19 : X-ray diffractograms of 25 sccm a-Si:H for different annealing temperatures

4.3.4. Optical Spectroscopy Results

The optical transmission spectra for the 5 sccm and 25 sccm a-Si:H as prepared samples and when annealed at 300^0C and 500^0C are presented in figures 4.20 and 4.21 respectively. The presence of the interference fringes and the intensity of peaks are the characteristics of thickness and the refractive index of the thin film. From the figures, it was observed that for both samples, the interference fringes at lower wavelength were broader than the interference fringes at the higher wavelengths. This was consistent with optical theory that the refractive index decreases with the wavelength and the graph usually follows the Cauchy rule. However, this observation showed that broad interference fringes indicated lower refractive index. This can be used to explain the spectrum further. It was observed that for the 5 sccm as prepared sample, the interference fringes at longer wavelengths were broader than that for the 25 sccm as prepared sample. This indicated that the static refractive index of the 5 sccm as prepared sample could be lower than the static refractive index of the 25 sccm as prepared sample. For the 5 sccm as prepared sample, it was also observed that the transmission intensity in the long wavelength region was high as compared to the 25 sccm as prepared sample. This observation suggested that the 25 sccm sample was more reflecting since absorption was minimum in this wavelength region. This strongly supported the above fact that the refractive index could be higher for the 25 sccm sample. Another notable observation is that for the 25 sccm as prepared sample, the maximum and minimum shifted towards the longer wavelength as compared to the 5 sccm as prepared sample. This observation indicated that the refractive index for the 25 sccm as prepared sample could be higher. From the transmission spectra for both samples, it was observed that the transmission intensity in the long wavelength region especially decreased when the samples

are annealed at 300^0C and 500^0C. This indicated annealing at higher temperatures resulted in the sample being more reflecting and thus as discussed earlier indicated higher refractive index. It was also observed that the position of respective maxima and minima shifted towards the longer wavelengths when the samples were annealed at higher temperatures, indicating that the refractive index increased within the whole spectrum when annealed at higher temperatures.

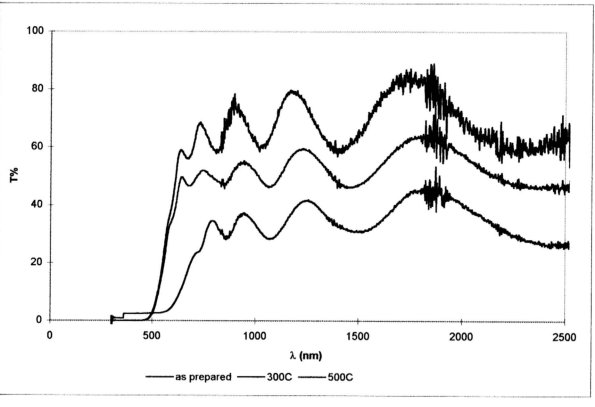

gure 4.20: Optical transmission spectrum of 5 sccm a-Si:H sample for various annealing temperature

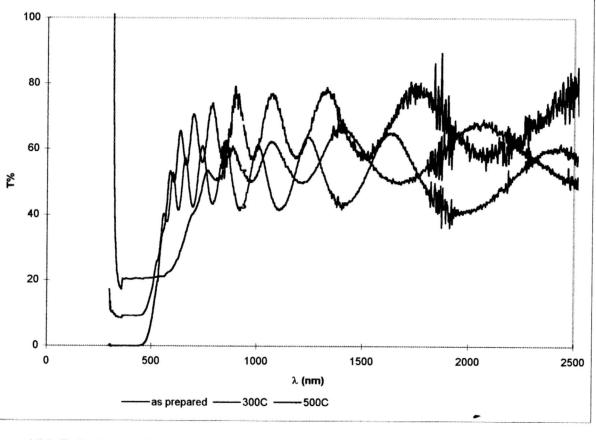

gure 4.21: Optical transmission spectrum of 25 sccm a-Si:H sample for various annealing temperature

Figures 4.22 and 4.23 show the dispersion curves i.e. refractive index (n) versus wavelength (λ) for the 5 sccm and 25 sccm as prepared samples and when annealed at 300^0C and 500^0C respectively. These curves were derived from the optical spectra (figures 4.20 and 4.21) using calculations discussed in section 3.4.1 (chapter 3). It was apparent that n decreased when λ increased and n saturates at longer wavelengths. From the plot of the dispersion curve, it was observed that the refractive index for 25 sccm as prepared sample was higher then in 5 sccm as prepared sample within the spectrum region. This observation indicated that the surface reflectivity and scattering in the 25 sccm as prepared sample was higher. When both samples were annealed at 300^0C and 500^0C, the refractive index for both samples increased.

Figures 4.24 and 4.25 illustrate a plot of $1/(n^2-1)$ versus E for both as prepared and annealed samples. From the figures, the variation in the gradient of these slopes were not significant but the intercepts of these plots with $1 / (n^2 - 1)$ axis were different for the for 5 sccm and 25 sccm samples. The intercept was observed to be higher 5 sccm sample. When annealed at 300^0C, the intercept position decreased significantly for both the samples. The decrease in the intercept position were smaller when samples were annealed at 500^0C. However the decrease was significantly larger for the 25 sccm sample. The slopes and the intercepts will be used in the next chapter to determine the hydrogen content in the film .

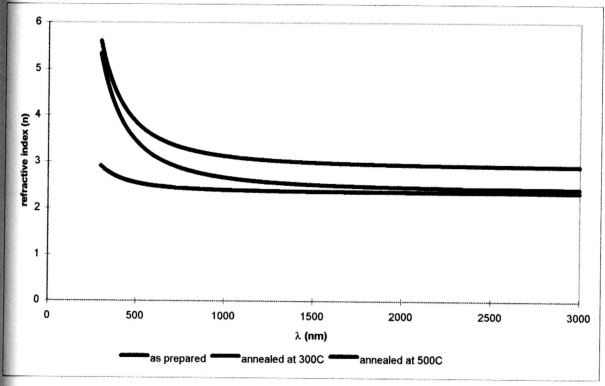

Figure 4.22: Variation of n as a function of wavelength for 5 sccm sample at various annealing temperatures

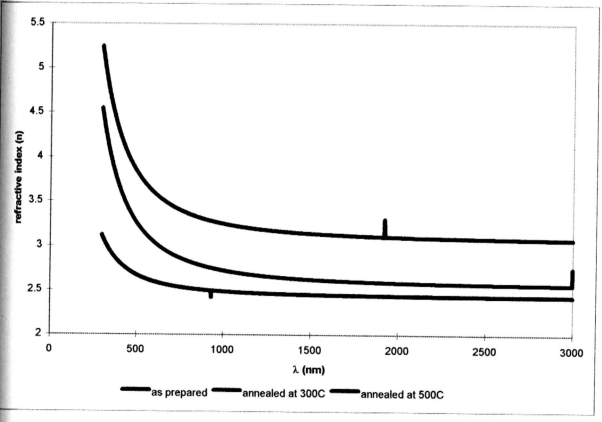

Figure 4.23: Variation of n as a function of wavelength for 25 sccm sample at various annealing temperatures

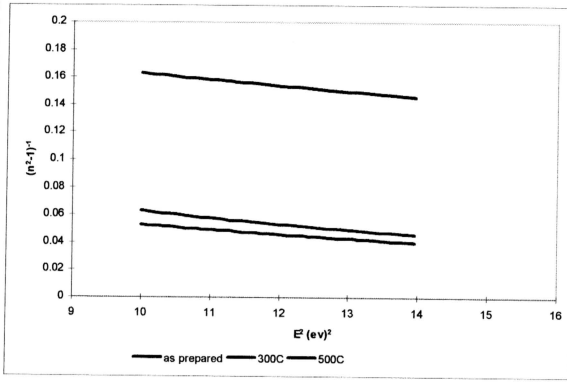

Figure 4.24: Variation of $1/(n^2-1)$ as a function of E for 5 sccm sample at various annealing temperatures

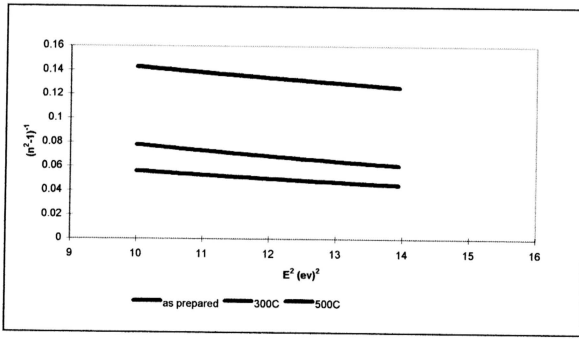

Figure 4.25: Variation of $1/(n^2-1)$ as a function of E for 25 sccm sample at various annealing temperatures

The absorption coefficient (α) was obtained from the transmission data by using equation 3.28 (presented in chapter III). From this absorption coefficient data at various wavelengths, a typical Tauc plot [88] was constructed to obtain the optical energy gap (E_g). For most amorphous films, the densities of states at the valence and conduction band edges are assumed to have a parabolic dependence on energy. According to the power law used in the absorption region, with this dependence the optical gap can be determined using the a Tauc's plot viz. $(\alpha E)^{1/2}$ versus E where α is the absorption coefficient and E is the photon energy [89]. From fig. 4.26, it was observed that the 5 sccm as prepared sample and the sample annealed at 300^0C produced linear plots in this region indicating that the densities of states of the valence and conduction band edges have parabolic dependence. However, when the sample was annealed at 500^0C linear plots could not be obtained in this region. This indicated that the densities of states at the valence and conduction band edges were not parabolic in nature and using the power law in the absorption edge, the density of states at the band edges were deduced to be constant. To obtain the E_g for this sample, a plot of (αE) versus E was next obtained as shown in fig. 4.27 and the E_g was obtained from the linear region of the plot. From the fig. 4.28, it was observed that only the Tauc's plot for the 25 sccm as prepared sample produced a linear region indicating that the densities of states has parabolic dependencies on energy whereas the samples annealed at 300^0C and 500^0C showed no linear region, again indicating that the densities of states are constant at the valence and conduction band edges. To obtain the E_g for both these samples, the (αE) versus E plot was again used as shown in figure 4.29. From the Tauc's plot, it was observed that for the 5 sccm as prepared sample, the absorption edge shifted towards the lower energy as compared to the 25 sccm as prepared sample. This indicated that the E_g for 5 sccm as

prepared sample was lower. From the plot it was observed that, for both samples the absorption edges shifted towards lower energies as the samples were annealed at higher temperatures. This indicated that the energy gap of the sample which were annealed at higher temperatures decreased. The samples which were annealed at 300^0C showed a slight shift in the absorption edge indicating that the energy gap of the samples which were annealed at this temperature did not decrease significantly. However, when annealed at 500^0C a large significant shift in the absorption edge was observed indicating that the E_g of the samples decreased significantly.

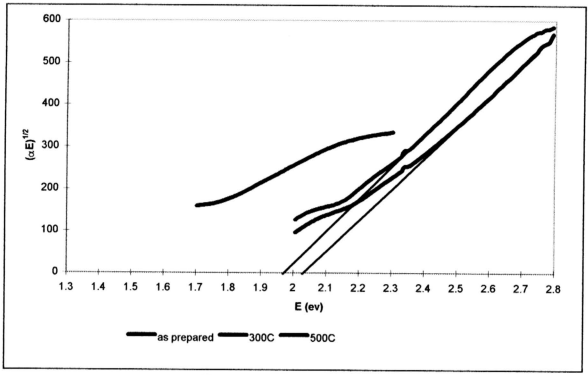

Figure 4.26: Variation of $(\alpha E)^{1/2}$ as a function of E for the 5sccm sample at various annealing temperature

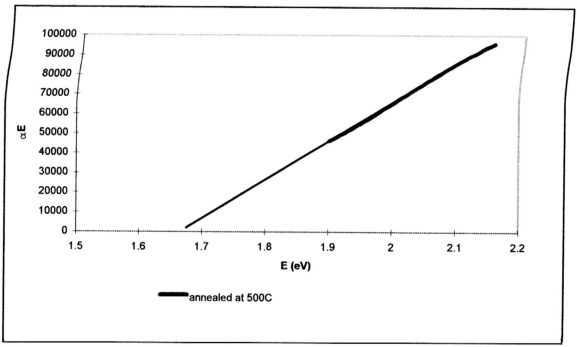

Figure 4.27 : Variation of (αE) as a function of E for 5 sccm sample annealed at 500^0C

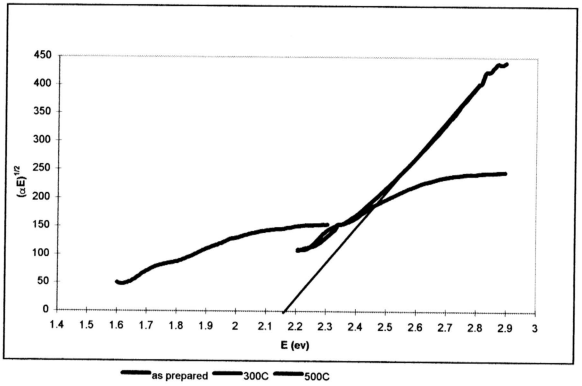

Figure 4.28: Variation of $(\alpha E)^{1/2}$ as a function of E for 25 sccm sample annealed at various annealing temperatures

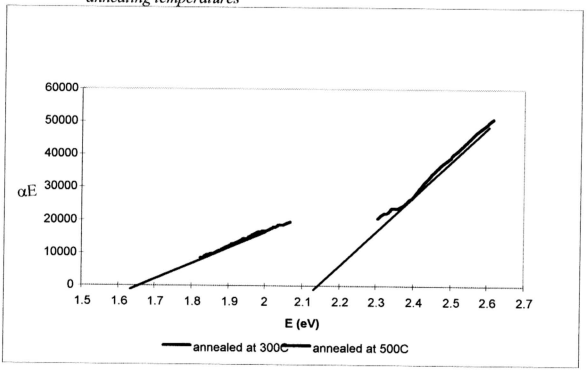

Figure 4.29: Variation of (αE) as a function of E for 25 sccm sample at various annealing temperatures

Figures 4.30 and 4.31 illustrate the plot of ln(α) versus photon energy(E) used to estimate Urbach Tail Band Width (E_e) for as prepared and annealed samples at 300^0C and 500^0C for both 5 sccm and 25 sccm flow-rates respectively. From the plots so obtained, it was observed that the gradient of the linear region in 5 sccm as prepared sample was higher than that of the 25 sccm as prepared sample. This indicates that the E_e for the 5 sccm sample was comparatively lower than that of the 25 sccm as prepared sample. From the graph, the slope of the plot in the linear region was obtained and the inverse of the slope provides E_e. Results indicate that the E_e for both samples increases when they are annealed at 300^0C and 500^0C. Increase in the Urbach Tail Band width indicates the increase in the disorder in the sample.

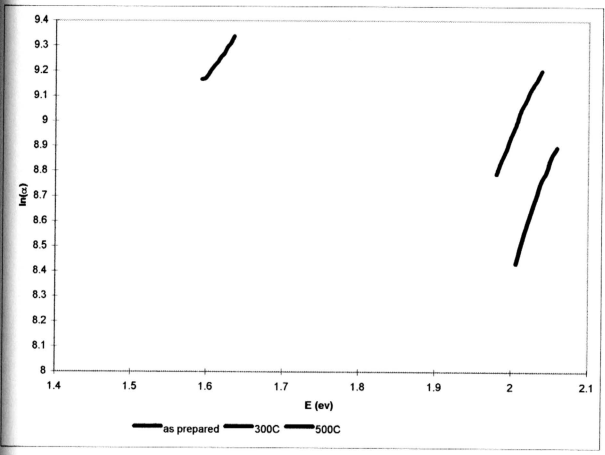

Figure 4.30: Variation of ln(α) as a function of E for 5 sccm sample at various annealing temperatures

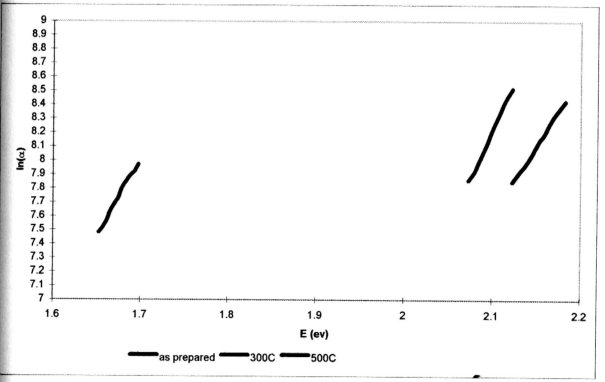

Figure 4.31: Variation of ln(α) as a function of E for 25 sccm sample at various annealing temperatures

4.3.5. Conductivity Measurements on a-Si:H

I) D.C. Electrical Characterisation Of a-Si:H

Figures 4.32 and 4.33 illustrate the current-voltage (I-V) plots for both 5 sccm and 25 sccm a-Si:H samples which were annealed at various annealing temperatures and the measurements were done at room temperature. For both these samples, the ohmic region lies between 50 volt - 90 volt and this was utilised in calculating the conductivity of the sample. The slope of the I-V plots for both as prepared samples, were almost the same. This indicates that the conductivity could be of the same order of magnitude. The slopes of the I-V plots were observed to increase with annealing temperature. Thus the conductivity of these samples can be expected to increase with the annealing temperature.

In this work, the I-V measurements were done for both samples at various temperatures which range from room temperature, 297^0K to 338^0K. This measurement was also done for the samples annealed at 300^0C and 500^0C. The conductivity at measured temperatures was determined for these samples. The plots of $\ln(\sigma)$ versus 1/T for the 5 sccm and 25 sccm as prepared samples and when annealed at 300^0C and 500^0C are presented in figure 4.34 and 4.35. These plots clearly show that the gradient of the slopes decreased with the annealing temperature indicating that the activation energy for both samples decreases when annealed at higher temperature. The actual values of the activation energies will be presented and analysed in the next chapter.

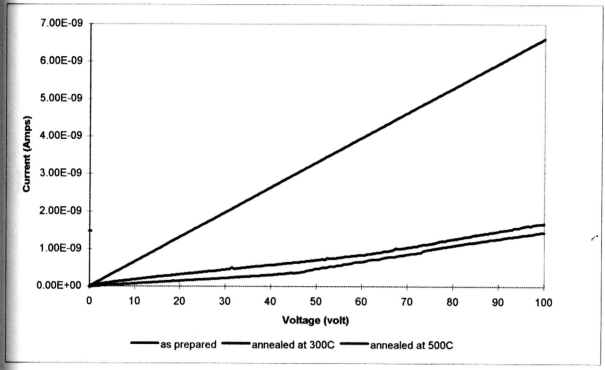

Figure 4.32 : Variation of voltage with current at room temperature for 5 sccm sample a-Si:H sample at different annealing temperature.

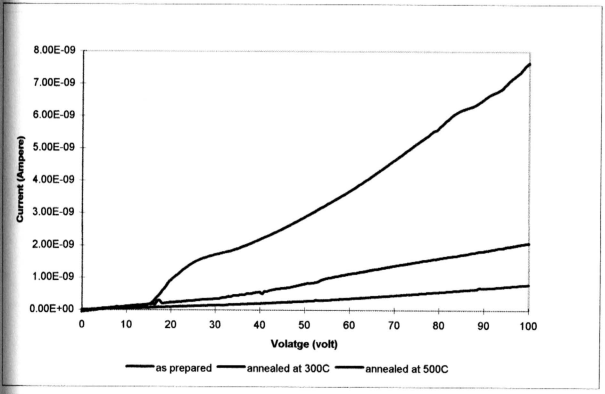

Figure 4.33 : Variation of voltage with current at room temperature for 25 sccm sample a-Si:H sample at different annealing temperature.

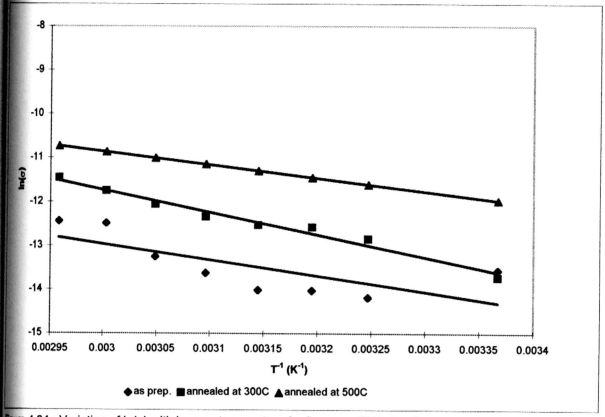

Figure 4.34 : Variation of ln(σ) with inverse temperature for 5 sccm a-Si:H at various annealing temperature

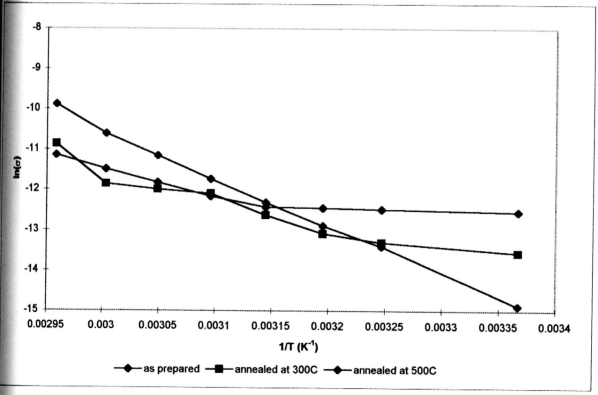

Figure 4.35: Variation of ln(σ) with inverse temperature for 25 sccm a-Si:H at various annealing temperature

II) A.C. Electrical Characterisation Of a-Si:H

Alternating current (a.c.) measurements (section 3.4.3) were carried out for the 5 sccm and 25 sccm samples studied in this work. The a-Si:H films studied were deposited on crystalline silicon and glass substrates. Figures 4.36 and 4.37 present the variation of parallel capacitance (C_p) as a function of frequency for the 5 sccm and 25 sccm a-Si:H samples on crystalline-Si substrate respectively. The effects of annealing on these samples can also be observed from these figures. These plots are used to determine the thickness of the thin film on the crystalline-Si. For this purpose the capacitance values in the high frequency region were used. For 5 sccm sample , the value of C_p for the sample annealed at 300^0C was lower as compared to the as prepared sample. The C_p increased when the sample was annealed at 500^0C. This suggested that annealing at 300^0C decreases the amount of charges in the film while annealing at 500^0C increases the amount of charges in the film. Annealing at 300^0C reduces the defects thus reducing the charges while unsatisfied bonds present when the sample was annealed at 500^0C due to the hydrogen evolution could have contributed to the increase in the amount of charges [90].

Figure 4.38 and 4.39 show the variations of C_p with frequency for both samples on the glass substrate in the as prepared and annealed at 300^0C and 500^0C conditions respectively. For the as prepared sample, the capacitance was lowest and saturated at very low frequency. The magnitude of the capacitance were of the same order of magnitude for both the samples. For the 5 sccm sample, the trend of the C_p versus frequency plot were similar for the as prepared sample and when the sample was annealed at 300^0C and 500^0C. The significant change observed was the increase in C_p when the sample was annealed at higher temperatures. The variation of C_p with frequency for the sample on crystalline silicon

substrate however did not show this increasing trend. For this sample, the C_p decreased when annealed at 300^{0}C. So the decrease in charges must not be due to the defect reduction in the a-Si:H but could be due to the defect reduction in the crystalline silicon which could be more dominant. For the 25 sccm sample the trend for the variation of C_p versus frequency is significantly different for the sample annealed at 300^{0}C. The capacitance increases with the frequency, reached a maximum at 2000 Hz and decreases again to a plateau at a frequency of 3000 Hz to 4000 Hz and further decreased as the frequency increased to 5000 Hz. This peculiar trend could not be explained.

Figures 4.40 and 4.41 present the conductance (G) versus frequency plots for the 5 sccm and 25 sccm as prepared samples and when annealed at 300^{0}C and 500^{0}C. The conductance increases with the frequency in a slow exponential trend for these plots except for the 5 sccm sample annealed at 500^{0}C. For the 5 sccm sample the increase was very steep. The increase in G with frequency is due to the hopping by carriers into localized states at the band edges and hopping of electrons at the fermi level. When the frequency increases, the hopping becomes more frequent thus increasing the G. The slopes for both samples increased when annealed at higher temperatures. This indicates that hopping conductivity increases when the samples are annealed at higher temperature. Increase in dangling bonds or defects in the samples increases the number of states in the gap and at the band edges thus making hopping conductivity more possible. The plot for $\sigma(\omega)$ at the frequency range 10^6 Hz for the 5 sccm and 25 sccm samples on glass substrate, as prepared and annealed at 300^{0}C and 500^{0}C were illustrated in figure 4.42 and 4.43. From these plots, the density of states at fermi level [$N(E_f)$] was obtained and has been presented in the next chapter.

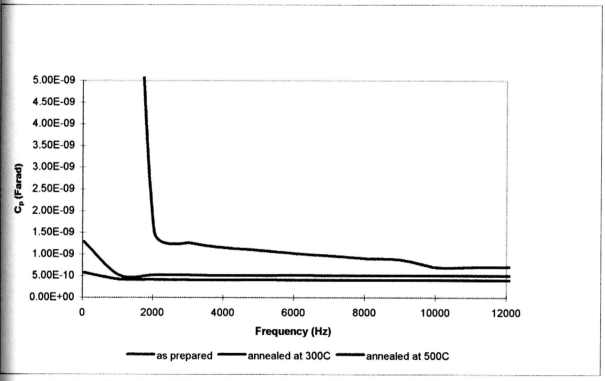

Figure 4.36 : Variation of parallel capacitance with frequency for various annealing temperature for 5sccm a-Si:H thin film on crystalline-Si substrate.

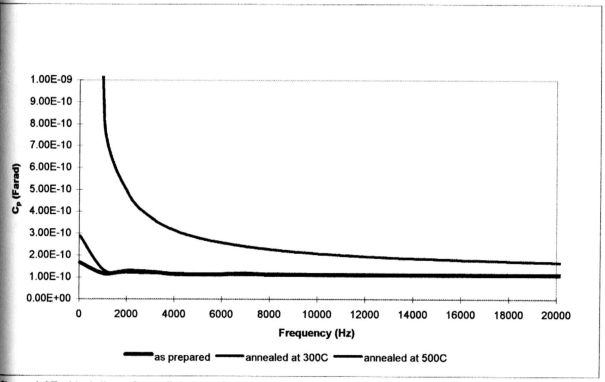

Figure 4.37 : Variation of parallel capacitance with frequency for various annealing temperature for 25sccm a-Si:H thin film on crystalline-Si substrate.

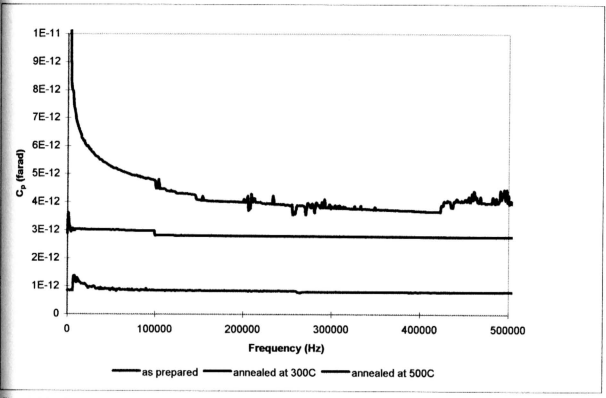

Fig . 4.38 : Frequency dependent of parallel capacitance at room temperature for 5sccm a-Si:H thin film on glass substrate at various temperatures annealing temperatures

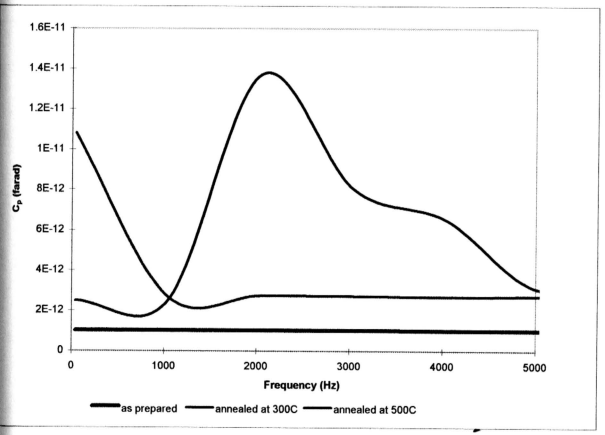

Fig . 4.39 : Frequency dependent of parallel capacitance at room temperature for 25sccm a-Si:H thin film on glass substrate at various temperatures annealing temperatures

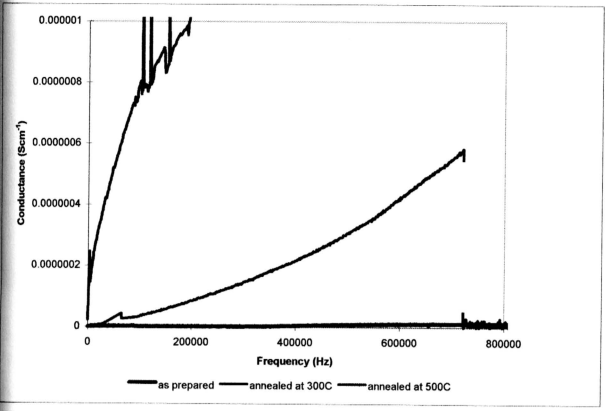

Fig . 4.40 : Frequency dependent of conductance at room temperature for 5sccm a-Si:H thin film on glass substrate at various temperatures annealing temperatures

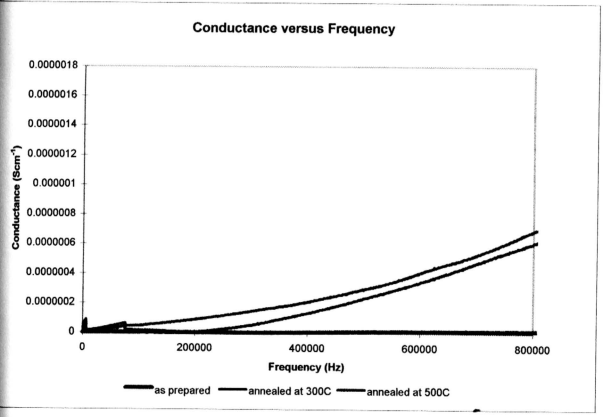

Fig . 4.41 : Frequency dependent of conductance at room temperature for 25sccm a-Si:H thin film on glass substrate at various temperatures annealing temperatures

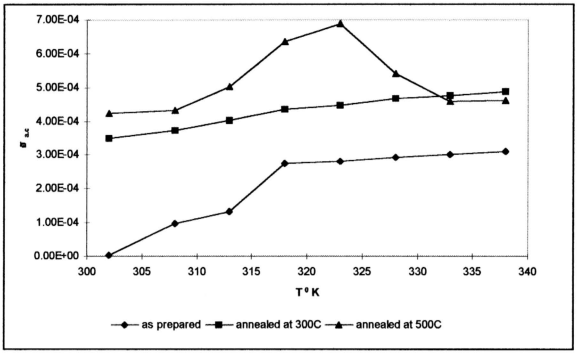

Figure 4.42: Variation in the a.c. conductivity with temperature for various annealing temperature for 5 sccm a-Si:H thin film on glass substrate at $\omega = 10^6$ Hz

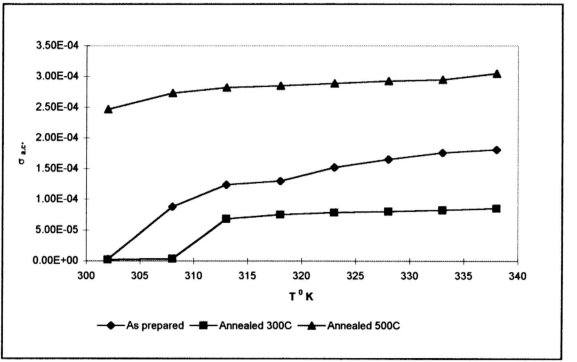

Figure 4.43: Variation in the a.c. conductivity with temperature for various annealing temperature for 25 sccm a-Si:H thin film on glass substrate at $\omega = 10^6$ Hz